doi:10.1093/jmcb/mjt012
Published online April 8, 2013

Article

Deletion of mouse *Alkbh7* leads to obesity

Anja Solberg[1], Adam B. Robertson[1,*], Jan Magnus Aronsen[2,3,4], Øivind Rognmo[5], Ivar Sjaastad[2,3], Ulrik Wisløff[5], and Arne Klungland[1,6,*]

[1] Clinic for Diagnostics and Intervention and Institute of Medical Microbiology, Oslo University Hospital, Rikshospitalet, 0027 Oslo, Norway
[2] Institute for Experimental Medical Research, Oslo University Hospital and University of Oslo, 0407 Oslo, Norway
[3] K.G. Jebsen Cardiac Research Center and Center for Heart Failure Research, University of Oslo, 0407 Oslo, Norway
[4] Bjørknes College, Oslo, Norway
[5] K.G. Jebsen Center of Exercise in Medicine, Department of Circulation and Medical Imaging, Faculty of Medicine, Norwegian University of Science and Technology, 7491 Trondheim, Norway
[6] Institute of Basic Medical Sciences, University of Oslo, 0315 Oslo, Norway
* Correspondence to: Arne Klungland, Tel: +4723074072; Fax: +4723074061; E-mail: arne.klungland@rr-research.no; Adam B. Robertson, Tel: +4723073119; Fax: +4723074061; E-mail: adam.robertson@rr-research.no

Mammals have nine homologues of the *Escherichia coli* AlkB repair protein: Alkbh1–8, and the fat mass and obesity associated protein FTO. In this report, we describe the first functional characterization of mouse Alkbh7. We show that the Alkbh7 protein is located in the mitochondrial matrix and that an *Alkbh7* deletion dramatically increases body weight and body fat. Our data indicate that Alkbh7, directly or indirectly, facilitates the utilization of short-chain fatty acids, which we propose is the likely cause for the obesity phenotype observed in the *Alkbh7*$^{-/-}$ mice. Collectively, our data provide the first direct demonstration that murine Alkbh7 is a mitochondrial resident protein involved in fatty acid metabolism and the development of obesity.

Keywords: AlkB, Alkbh7, fatty acid oxidation, mitochondria, obesity

Introduction

Escherichia coli AlkB was discovered nearly 30 years ago as a gene that could confer resistance to alkylating reagents (Kataoka et al., 1983). Two decades later, AlkB was classified as a member of the 2-oxoglutarate and iron-dependent dioxygenase superfamily (Aravind and Koonin, 2001) and was shown to repair alkylated DNA via oxidative demethylation (Falnes et al., 2002; Trewick et al., 2002). Nine AlkB homologues have been identified in mammals—Alkbh1–8 (Wei et al., 1996; Duncan et al., 2002; Kurowski et al., 2003), and the fat mass and obesity-associated FTO (Gerken et al., 2007). AlkB homologues 2 and 3 have similar biochemical activity as the *E. coli* AlkB (Duncan et al., 2002; Ringvoll et al., 2006, 2008; Dango et al., 2011). Null mice for Alkbh1 indicate roles of this homologue in lineage differentiation, epigenetic regulation, and histone H2A hydroxylation (Pan et al., 2008; Nordstrand et al., 2010; Ougland et al., 2012), while ALKBH5, ALKBH8, and FTO are required for introducing and reversing modifications in various RNA species (Fu et al., 2010; Songe-Moller et al., 2010; Jia et al., 2011; van den Born et al., 2011; Zheng et al., 2013; Berulava et al., 2013). The ninth AlkB homologue, FTO, has been linked to obesity in both humans (Dina et al., 2007; Frayling et al., 2007; Sovio et al., 2011) and mice (Church et al., 2009, 2010; Fischer et al., 2009; McMurray et al., 2013). However, the mechanism by which FTO affects obesity is unknown (Stratigopoulos and Leibel, 2010; Larder et al., 2011). Obesity and its associated disorders are some of the most pressing health issues facing medicine today (Kelly et al., 2008). In recent studies, considerable attention has been directed to unravel the molecular mechanisms that control the biology during obesity, thus contributing to the development of therapeutic strategies for obesity and the related pathologies, such as diabetes (Ma et al., 2012). There appears to be substantial individual variation among the obese population, reflecting genetic and epigenetic differences that either protects the populace from or exacerbates the development of obesity (Hetherington and Cecil, 2010).

We established an *Alkbh7* knockout (*Alkbh7*$^{-/-}$) mouse model to gain a better understanding of the previously unknown physiological role of *Alkbh7*. We show that Alkbh7 is a mitochondrial matrix resident protein that when deleted leads to dramatically increased body weight and body fat, a phenotype that is amplified when the mice are challenged with a high-fat diet (HFD). We provide evidence that suggests a role for Alkbh7 in the metabolism of short-chain fatty acids and demonstrates the downstream effects of aberrant fat metabolism in the *Alkbh7*$^{-/-}$ mice.

Received January 9, 2013. Revised March 5, 2013. Accepted March 19, 2013.

Results

Alkbh7 localizes to the mitochondrial matrix and is expressed in multiple tissues

Primary analysis of the Alkbh7 protein sequence using Mitoprot II (Claros and Vincens, 1996) suggested that Alkbh7 had a 92% probability of localizing to the mitochondria. Analysis of mouse embryonic fibroblast (MEF) cells showed that the Alkbh7 protein is present in the cytoplasm and colocalizes with mitochondrial cytochrome *c* (Figure 1A). Western blot analysis of mitochondrial protein extracts demonstrated that the extract was free from detectable levels of cytosolic and nuclear contaminants and that the Alkbh7 protein is present in the mitochondria (Figure 1B). Further fractionation of the mitochondria revealed that Alkbh7 is present in the mitochondrial matrix and not in the mitochondrial inner membrane (Figure 1C). These data, taken together, support the notion that Alkbh7 localizes to the mitochondria. Analysis of the mRNA expression pattern of *Alkbh7* showed expression in all tissues assayed (Figure 1D), suggesting a role for *Alkbh7* in multiple organs.

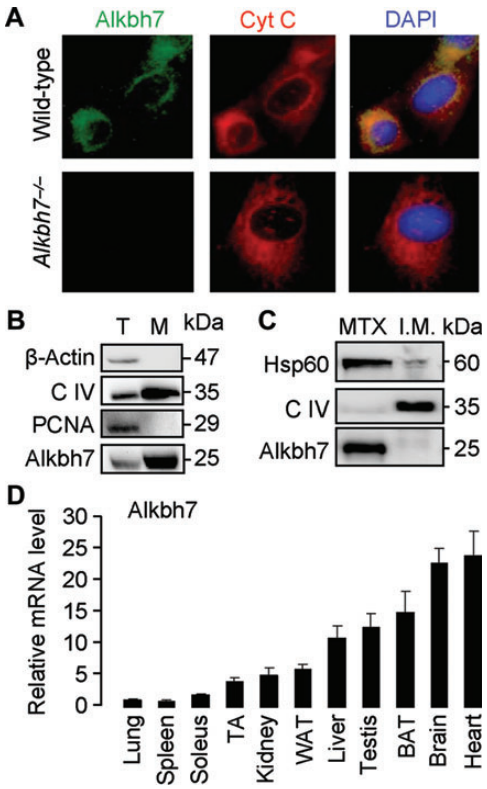

Figure 1 Alkbh7 is localized to the mitochondrial matrix. (**A**) Immunofluorescence analysis of the sub-cellular localization of Alkbh7 in MEF cells. Green, Alkbh7; red, mitochondrial marker cytochrome *c* (Cyt C); blue, 4′,6-diamidino-2-phenylindole (DAPI); *Alkbh7*$^{-/-}$, *Alkbh7* knockout MEFs. (**B**) Mitochondrial (M) and total cell (T) protein extracts probed using antisera directed against Alkbh7, proliferating cell nuclear antigen (PCNA), β-actin, and complex IV (C IV). (**C**) Soluble mitochondrial matrix (MTX) and mitochondrial inner membrane (I.M.) protein extracts probed with antisera for Alkbh7, α-heat-shock protein 60 (Hsp60), and Complex IV (C IV). (**D**) Relative *Alkbh7* mRNA levels in the indicated mouse tissues ($n = 3$). BAT, brown adipose tissue; WAT, white adipose tissue; TA, tibialis anterior. Data are expressed as mean ± SEM.

Generation of Alkbh7$^{-/-}$ *mice*

We generated *Alkbh7*$^{-/-}$ mice by deleting exons 2–4 of the *Alkbh7* gene to investigate the *in vivo* role of *Alkbh7* (Figure 2A). Exons 2–4 in the *Alkbh7* gene encode the conserved—and likely catalytic—2-oxoglutarate and iron-dependent dioxygenase AlkB domain. The detailed strategy using the Cre-lox system for the *Alkbh7* deletion is described in the Supplementary Materials and methods and is shown in Supplementary Figure S1A and B. The successful deletion of the *Alkbh7* gene was confirmed by western blot analysis and PCR (Supplementary Figure S1C).

Alkbh7$^{-/-}$ *mice have increased body weight relative to wild-type mice*

The mitochondrial localization of Alkbh7 led us to hypothesize that the metabolism and body weight of the *Alkbh7*$^{-/-}$ mice could be affected. Metabolism-related phenotypes have been shown to vary between the sexes and are thought to be due to differences in the hormonal profile of males and females (Gui et al., 2004; Wang et al., 2006; Macotela et al., 2009). Therefore, we grouped each genotype by gender to investigate potential metabolic Alkbh7-dependent differences between the sexes. *Alkbh7*$^{-/-}$ and wild-type mice were fed a standard chow diet (SD, 5.5% fat content) and weighed monthly from 1 month of age to 12 months of age. Male *Alkbh7*$^{-/-}$ mice weighed significantly more than their wild-type counterparts at all time points measured (Figure 2B). Female *Alkbh7*$^{-/-}$ mice showed increased body weight relative to female wild-type mice from 1 month of age; however, this weight difference was not statistically significant until 6 months of age (Figure 2C). Furthermore, analysis of the voluntary activity level showed that *Alkbh7*$^{-/-}$ mice were 37% less active compared with wild-type mice as measured by open field tests (Figure 2D).

Alkbh7$^{-/-}$ *mice are less resistant to weight-gain on an HFD than wild-type mice*

Four-month-old *Alkbh7*$^{-/-}$ and wild-type mice were fed an HFD (45% fat content) for 2 months to test if the increased chow fat content would amplify the observed weight phenotype. The weight of male *Alkbh7*$^{-/-}$ mice increased significantly relative to wild-type male mice from Week 4 on the HFD (Figure 3A), whereas female *Alkbh7*$^{-/-}$ mice displayed a dramatic weight gain after 1 week of eating the HFD compared with wild-type female mice fed the HFD (Figure 3B). Examination of the liver and heart of the *Alkbh7*$^{-/-}$ mice showed that these organs were both significantly heavier in the *Alkbh7*$^{-/-}$ mice relative to wild-type mice (Figure 3C and D). Furthermore, necropsy of male and female *Alkbh7*$^{-/-}$ mice fed the HFD revealed extensive fat deposits in the abdominal cavity (Figure 3E and F), suggesting that adipose tissue was the cause of the increased weight in the *Alkbh7*$^{-/-}$ mice.

Alkbh7$^{-/-}$ *mice have increased levels of body fat and larger adipose cells*

The body fat levels of wild-type and *Alkbh7*$^{-/-}$ mice were quantified using dual energy X-ray absorptiometry (DEXA). At 4 months of age, we found that female *Alkbh7*$^{-/-}$ mice have significantly more body fat relative to wild-type mice when fed the SD (Figure 4A). This increase in body fat was more striking when the mice were fed the HFD for 2 months. A remarkable increase in body fat, ∼5 g, was observed in *Alkbh7*$^{-/-}$ male and female

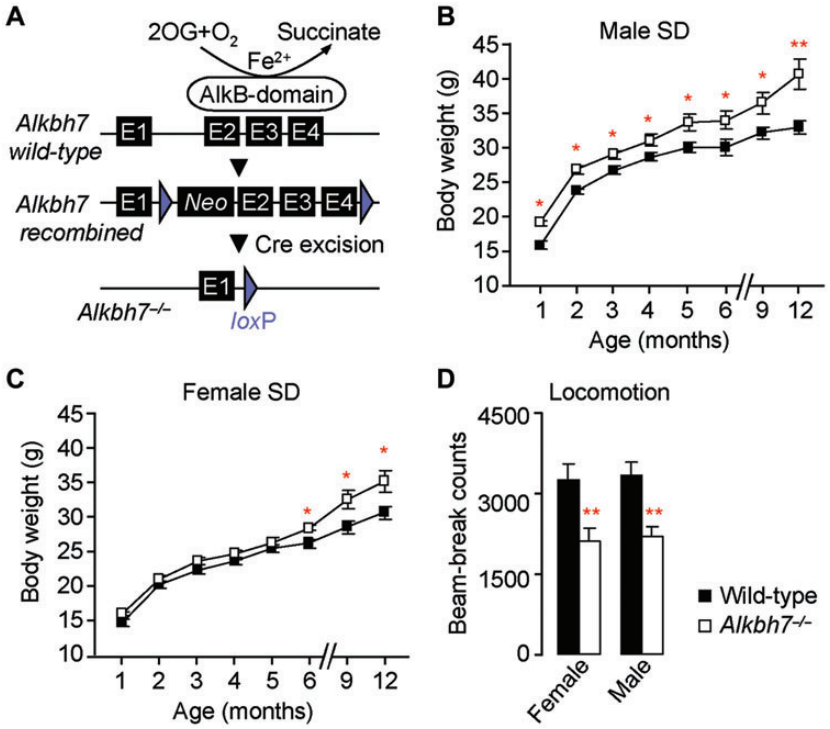

Figure 2 *Alkbh7*$^{-/-}$ mice weigh more and are less active than wild-type mice. (**A**) Structure of the *Alkbh7* wild-type locus, the *Alkbh7* recombined locus, and the *Alkbh7*$^{-/-}$ Cre excised knockout locus (*Alkbh7*$^{-/-}$). Exons 2–4 (E2–E4) encode the AlkB domain. Neo, *Neomycin* resistance gene; loxP, sites for Cre-mediated excision of exons 2–4; 2OG, 2-oxoglutarate. The figure is not to scale. (**B** and **C**) Body weight of male and female *Alkbh7*$^{-/-}$ and wild-type mice fed an SD until 12 months of age ($n = 14$). (**D**) Voluntary locomotion as measured by open-field tests. Wild-type, $n = 16$; *Alkbh7*$^{-/-}$, $n = 20$. Data are expressed as mean ± SEM. *$P < 0.05$, **$P < 0.01$.

mice relative to wild-type mice (Figure 4A). Lean mass was significantly lower in male *Alkbh7*$^{-/-}$ mice compared with male wild-type mice when fed either the SD or the HFD (Figure 4B). We did not detect a difference in lean mass between the female *Alkbh7*$^{-/-}$ mice and the female wild-type mice (Figure 4B). A comparison of the body composition change over the period the mice were fed the HFD showed that fat percentage, fat mass, and body weight were all higher in the *Alkbh7*$^{-/-}$ female and male mice compared with the wild-type mice (Supplementary Figure S2A). Additionally, histological analysis of white adipose tissue harvested from mice fed the HFD for 2 months revealed that *Alkbh7*$^{-/-}$ mice had significantly larger adipocytes compared with wild-type mice (Figure 4C). These data confirmed our supposition that adipose tissue was the main component of the increased body weight in the *Alkbh7*$^{-/-}$ mice.

Alkbh7$^{-/-}$ *mice are hypophagic on an HFD*

Obesity can be caused by excess caloric intake (Bray et al., 2010). Therefore, we investigated if the increased body fat in the *Alkbh7*$^{-/-}$ mice relative to wild-type mice was the result of increased food intake. Surprisingly, food intake data obtained from three time points during the HFD feeding regimen ($t = 2$ weeks, 1 month, and 2 months) showed that female and male *Alkbh7*$^{-/-}$ mice eat significantly less on an HFD compared with wild-type mice (Figure 4D and Supplementary Figure S2B). The difference in food intake was only associated with the HFD as we found no significant differences between *Alkbh7*$^{-/-}$ and wild-type mice when these mice were fed an SD ($t = 0$) (Figure 4D and Supplementary Figure S2B).

Alkbh7$^{-/-}$ *mice display a hormonal profile consistent with obesity*

Consistent with a direct correlation of leptin levels and body fat levels (Frederich et al., 1995), we found higher leptin levels in *Alkbh7*$^{-/-}$ female and male mice relative to wild-type mice after 2 months on the HFD (Table 1). Furthermore, female *Alkbh7*$^{-/-}$ mice had significantly lower levels of adiponectin compared with wild-type female mice (Table 1). Adiponectin is secreted by adipose tissue and its presence is inversely correlated with adipose tissue mass (Coll et al., 2007). However, the adiponectin levels were similar in the male *Alkbh7*$^{-/-}$ and wild-type mice, indicating a sex-dependent adiponectin profile in the *Alkbh7*$^{-/-}$ mice. We found no significant differences in the fasting serum levels of total cholesterol or triglycerides in *Alkbh7*$^{-/-}$ mice compared with wild-type mice; however, we found that both male and female *Alkbh7*$^{-/-}$ mice on the HFD regimen showed significantly higher fasting insulin levels compared with wild-type mice fed the HFD (Table 1).

Alkbh7$^{-/-}$ *mice have altered levels of circulating acylcarnitines*

The high *Alkbh7*$^{-/-}$ body fat levels and the mitochondrial localization of the Alkbh7 protein suggested that Alkbh7 could be involved in mitochondrial fatty acid oxidation. Therefore, lipid-derived metabolites were evaluated using tandem mass spectrometry of circulating acylcarnitine species (Haynes, 2011) to compare the profile of mitochondrial fatty acid metabolism in *Alkbh7*$^{-/-}$ mice to wild-type mice. The fed state profiles showed significantly higher levels of long-chain acylcarnitines and the short-chain C4-OH and C2 (acetyl-CoA) acylcarnitines in the *Alkbh7*$^{-/-}$ mice, while the C3 acylcarnitine level was nearly half the concentration

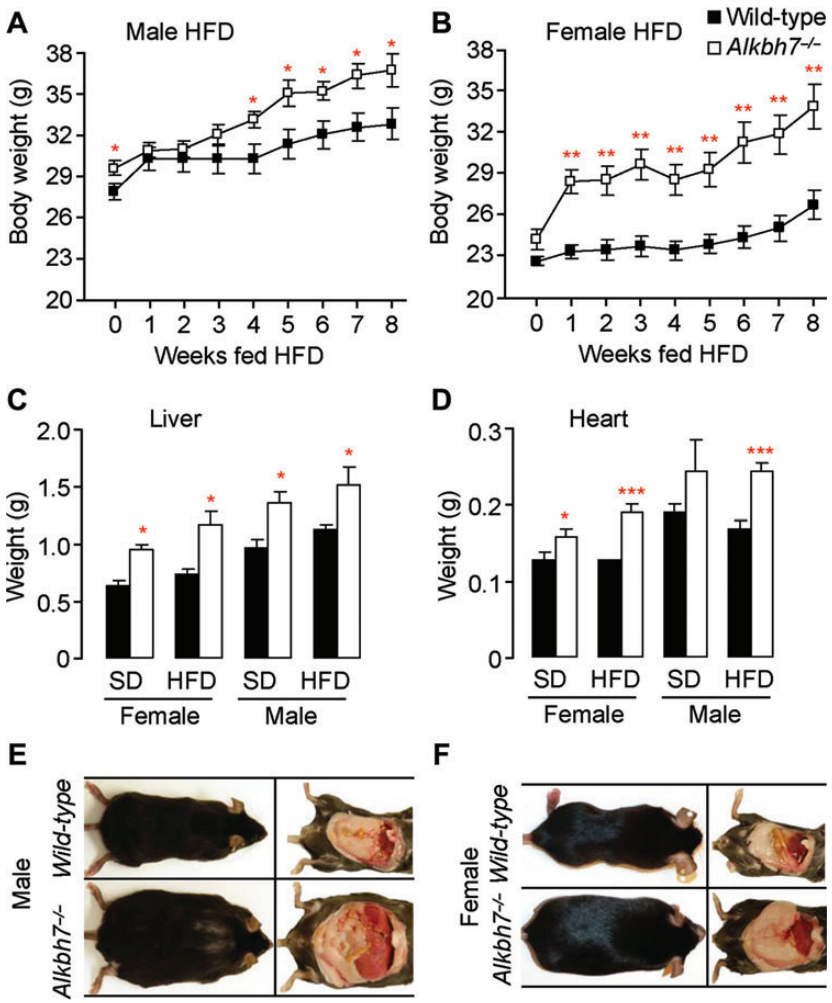

Figure 3 *Alkbh7*$^{-/-}$ mice have increased body weight when fed an HFD. (**A** and **B**) Body weight of male and female *Alkbh7*$^{-/-}$ and wild-type mice fed an HFD for 8 weeks ($n = 10$). (**C** and **D**) Liver and heart weights of *Alkbh7*$^{-/-}$ and wild-type mice fed an SD or an HFD ($n = 6$). (**E** and **F**) Representative postmortem pictures of male and female *Alkbh7*$^{-/-}$ and wild-type mice after an HFD. HFD, high-fat diet; SD, standard diet. Data are expressed as mean ± SEM. *$P < 0.05$, **$P < 0.01$, ***$P < 0.001$.

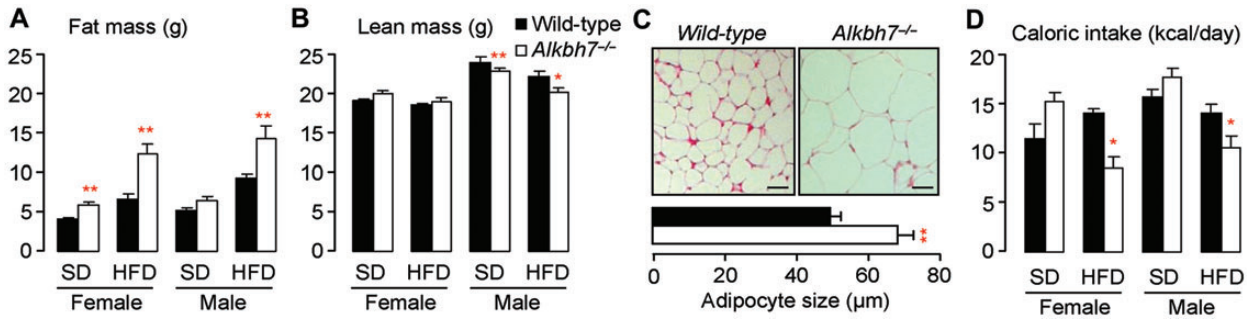

Figure 4 *Alkbh7*$^{-/-}$ mice have higher body fat levels and reduced food intake on an HFD. (**A** and **B**) Fat and lean mass in *Alkbh7*$^{-/-}$ and wild-type mice fed an SD or an HFD ($n = 10$). (**C**) Representative H&E staining and average adipocyte size of abdominal white adipose tissue from *Alkbh7*$^{-/-}$ and wild-type mice after the HFD. $n = 300$ cells from three sections from four mice. Scale bar, 50 μm. (**D**) Caloric intake in *Alkbh7*$^{-/-}$ and wild-type mice ($n = 10$). SD, standard diet; HFD, high-fat diet. Data are expressed as mean ± SEM. *$P < 0.05$, **$P < 0.01$.

in the *Alkbh7*$^{-/-}$ mice compared with wild-type mice (Figure 5A). The opposite situation manifested itself during fasting; all acylcarnitine species were reduced in the *Alkbh7*$^{-/-}$ mice compared with wild-type mice, with the exception of C3 and C4 acylcarnitines (Figure 5B). Figure 5C shows that after fasting, wild-type C3 and C4 acylcarnitine levels were reduced to nearly half the concentration measured in the fed state. *Alkbh7*$^{-/-}$ C3 and C4 acylcarnitine levels were unaltered in the fasted state relative to the fed state (Figure 5C). These data indicate aberrant fatty acid metabolism in the *Alkbh7*$^{-/-}$ mice. Oxidation of fatty acids generates ketones

Table 1 Metabolic parameters in overnight fasted *Alkbh7*$^{-/-}$ and wild-type mice.

	SD		HFD	
	Wild-type	*Alkbh7*$^{-/-}$	Wild-type	*Alkbh7*$^{-/-}$
Females				
Adiponectin (μg/ml)	5.65 ± 0.01	6.84 ± 0.20	7.06 ± 0.03	4.11 ± 0.05*
Leptin (ng/ml)	2.78 ± 0.07	5.53 ± 0.09	3.94 ± 0.12	12.8 ± 0.03**
Cholesterol (mg/dl)	100 ± 0.00	100 ± 0.00	104 ± 2.60	127 ± 11.8
Triglyceride (mg/dl)	50.0 ± 0.00	57.0 ± 3.72	51.9 ± 1.63	50.0 ± 0.00
Insulin (ng/ml)[a]	0.20 ± 0.04	0.26 ± 0.10	0.26 ± 0.05	0.51 ± 0.08*
Males				
Adiponectin (μg/ml)	3.08 ± 0.03	3.79 ± 0.04	3.25 ± 0.04	4.19 ± 0.08
Leptin (ng/ml)	3.21 ± 0.01	3.08 ± 0.06	5.51 ± 0.08	10.1 ± 0.11*
Cholesterol (mg/dl)	100 ± 0.00	104 ± 3.60	135 ± 8.00	110 ± 9.63
Triglyceride (mg/dl)	50.0 ± 0.00	55.8 ± 3.28	50.0 ± 0.00	50.0 ± 0.00
Insulin (ng/ml)[a]	0.46 ± 0.09	0.67 ± 0.12	0.37 ± 0.07	0.58 ± 0.06*

Data are expressed as mean ± SEM. SD, standard diet; HFD, high-fat diet. [a]Five hours fasting. *$P < 0.05$, **$P < 0.01$. $n = 6–8$ mice.

that can be used as an energy source; therefore, we analyzed fasting ketone levels. We were not able to detect a difference in the circulating levels of the ketone body β-hydroxybutyrate in the *Alkbh7*$^{-/-}$ mice compared with wild-type mice (Figure 5D), indicating that the altered fatty acid oxidation in the *Alkbh7*$^{-/-}$ mice does not affect ketogenesis.

Alkbh7$^{-/-}$ *deletion does not result in systemic lowering of amino acids*

As identified above, the circulating acylcarnitine profile in the *Alkbh7*$^{-/-}$ mice is indicative of a fatty acid oxidation defect in these mice. Therefore, we analyzed whether alternative carbon sources such as amino acids could be necessary for sufficient energy generation during fasting in the *Alkbh7*$^{-/-}$ mice. Using tandem mass spectrometry we were unable to detect a significant difference in the amino acid levels between wild-type mice and *Alkbh7*$^{-/-}$ mice (Supplementary Figure S3A and B), indicating that *Alkbh7*$^{-/-}$ mice are not using amino acids as an alternative energy source.

Alkbh7$^{-/-}$ *mice are not glucose intolerant and have increased glycogen stores*

We hypothesized that the *Alkbh7*$^{-/-}$ mice were able to store and utilize glucose as an energy source more efficiently than wild-type mice. As glucose tolerance is often reduced in obese individuals, we were surprised to find that the glucose tolerance of the *Alkbh7*$^{-/-}$ mice was similar to that of wild-type mice fed the HFD. In fact, the female *Alkbh7*$^{-/-}$ mice showed a trend of improved glucose tolerance relative to the wild-type mice (Figure 6A). Furthermore, upon injection of insulin, *Alkbh7*$^{-/-}$ females responded with a significant decrease in glucose levels relative to wild-type females (Figure 6B), contrasting with the reduced insulin sensitivity typically observed in obese individuals (Kahn et al., 2006). We were not able to detect significant differences in the glucose and insulin tolerance between the male *Alkbh7*$^{-/-}$ and wild-type mice (Supplementary Figure S4A and B). However, we noted that both male and female *Alkbh7*$^{-/-}$ mice fed the SD had significantly lower glucose levels after overnight fasting compared with wild-type mice (Figure 6C), indicating increased glucose utilization by the *Alkbh7*$^{-/-}$ mice during fasting relative to wild-type mice. Furthermore, fasting glycogen levels were significantly increased in the *Alkbh7*$^{-/-}$ liver compared with wild-type liver, demonstrating abnormally high storage levels of glycogen in the *Alkbh7*$^{-/-}$ mice (Figure 6D).

Alkbh7$^{-/-}$ *mitochondria show increased respiration when using carbohydrates*

Based on the glucose homeostasis data we wanted to address whether *Alkbh7*$^{-/-}$ mitochondria utilize carbohydrates more efficiently relative to wild-type mitochondria. Therefore, we evaluated the maximal and qualitative aspects of oxidative metabolism in wild-type and *Alkbh7*$^{-/-}$ mitochondria by the sequential addition of palmitoyl-carnitine, pyruvate, glutamate, and succinate (Figure 6E). We did not find any respiratory differences using palmitoyl-carnitine (long-chain acylcarnitine) as substrate, while the mitochondrial respiratory capacities using pyruvate and glutamate as substrates were, respectively, 19% and 22% higher in *Alkbh7*$^{-/-}$ mitochondria relative to wild-type mitochondria. Furthermore, we noted that the increased respiratory capacity in *Alkbh7*$^{-/-}$ mitochondria relative to wild-type mitochondria using succinate as a substrate was close to statistical significance ($P = 0.056$). The increase in the *Alkbh7*$^{-/-}$ mitochondrial respiration with sugar substrates, but not with palmitoyl-carnitine, suggests that the *Alkbh7*$^{-/-}$ mitochondria have developed mechanisms to use carbohydrates more efficiently than wild-type mitochondria to compensate for aberrant fatty acid oxidation in the *Alkbh7*$^{-/-}$ mice.

Discussion

The *Alkbh7*$^{-/-}$ phenotype, which includes obesity and hormonal changes consistent with obesity, is indicative of a metabolic disorder present in these mice. Indeed, our data show that the deletion of *Alkbh7* leads to a dramatic increase in body fat, supporting a role for *Alkbh7* in fat metabolism. As the Alkbh7 protein resides in the mitochondrial matrix, the causal factor of the changes observed in the *Alkbh7*$^{-/-}$ mice likely originates from within the mitochondria. Furthermore, as Alkbh7 is expressed in all tissues assayed, Alkbh7 most likely has a generalized role in mitochondrial metabolism. The mitochondrial localization of Alkbh7 contrasts with a previous study showing a diffuse localization pattern of Alkbh7 in human cells (Tsujikawa et al., 2007). We believe that the N-terminal GFP-tag on the Alkbh7 protein analyzed by Tsujikawa et al. (2007) blocked the N-terminal mitochondrial localization signal of Alkbh7, thus creating the diffuse signal observed in their localization assay.

Our acylcarnitine data suggest that the *Alkbh7*$^{-/-}$ mice do not initiate β-oxidation as readily as wild-type mice in the fed state, demonstrated by the higher levels of long-chain acylcarnitine species in the *Alkbh7*$^{-/-}$ mice. The reduced levels of the short-chain acylcarnitines C3 and C4 in the fed state indicate that the *Alkbh7*$^{-/-}$ mice are utilizing resources other than acylcarnitines for energy production. In line with this hypothesis, we propose that the short-chain acylcarnitines are metabolized to the longer chain acylcarnitines, leading to the acylcarnitine profile demonstrated in the *Alkbh7*$^{-/-}$ mice. As a direct result of this, more

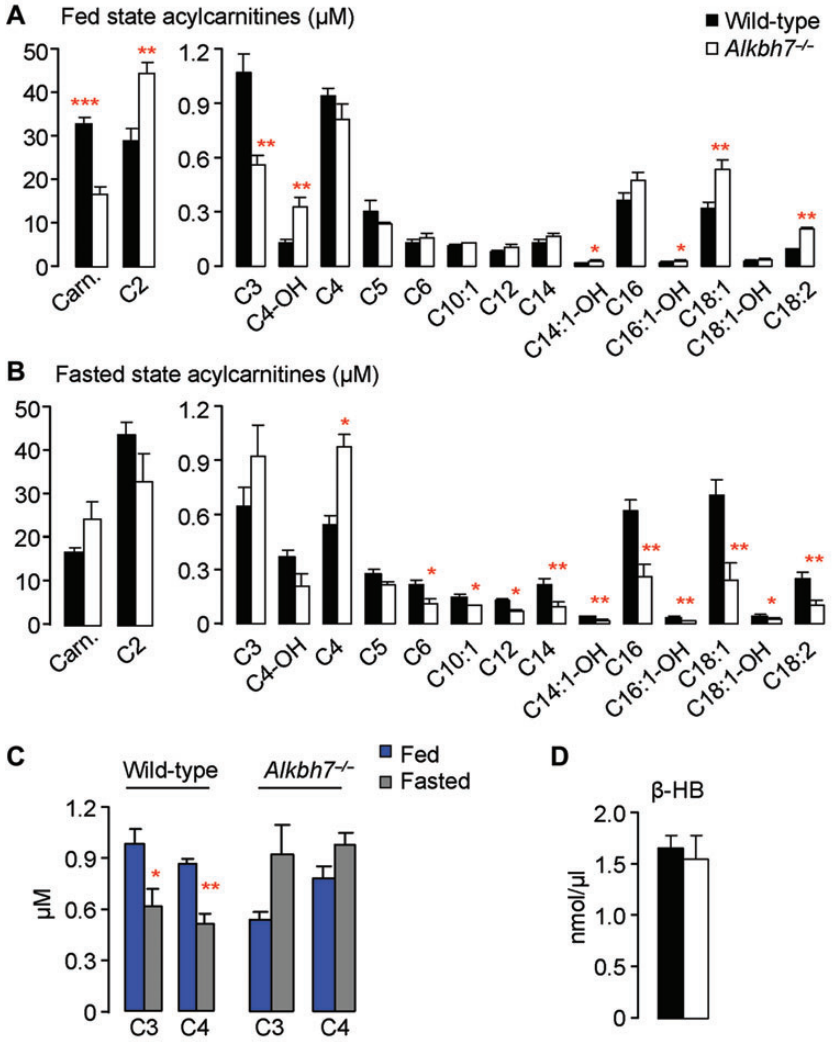

Figure 5 *Alkbh7*$^{-/-}$ mice have altered circulating acylcarnitine levels. (**A** and **B**) Fed and fasted state acylcarnitine profile in *Alkbh7*$^{-/-}$ plasma relative to wild-type plasma as analyzed by tandem mass spectrometry. Carn., free carnitine. (**C**) Comparison of C3 and C4 acylcarnitine levels in *Alkbh7*$^{-/-}$ and wild-type plasma during fed and fasted state. (**D**) Circulating β-hydroxybutyrate (β-HB) in overnight fasted *Alkbh7*$^{-/-}$ and wild-type mice. $n = 6$ for all experiments. Data are expressed as mean ± SEM. *$P < 0.05$, **$P < 0.01$, ***$P < 0.001$.

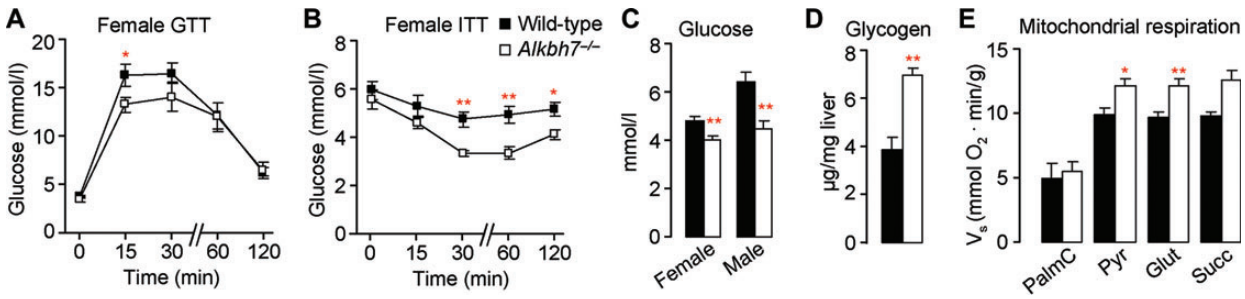

Figure 6 *Alkbh7*$^{-/-}$ mice display altered use and storage of carbohydrates. (**A** and **B**) Glucose tolerance test (GTT) and insulin tolerance test (ITT) in female *Alkbh7*$^{-/-}$ and wild-type mice fed an HFD ($n = 9$). (**C**) Fasting levels of circulating glucose in *Alkbh7*$^{-/-}$ and wild-type mice fed an HFD ($n = 9$). (**D**) Fasting liver glycogen levels from female *Alkbh7*$^{-/-}$ and wild-type mice fed an SD ($n = 3$). (**E**) *Alkbh7*$^{-/-}$ and wild-type mitochondrial substrate utilization and respiration using a Clark electrode. PalmC, Palmitoyl-carnitine; Pyr, pyruvate; Glut, glutamate; Succ, succinate. $n = 12$. Data are expressed as mean ± SEM. *$P < 0.05$, **$P < 0.01$.

fatty acids are stored as fat, leading to the obesity phenotype observed in the *Alkbh7*$^{-/-}$ mice. During fasting, when the reliance upon fatty acids for energy production increases, it appears that *Alkbh7*$^{-/-}$ mice do initiate β-oxidation as demonstrated by the lower levels of medium- and long-chain acylcarnitines compared with wild-type mice. However, the abnormal accumulation of C3

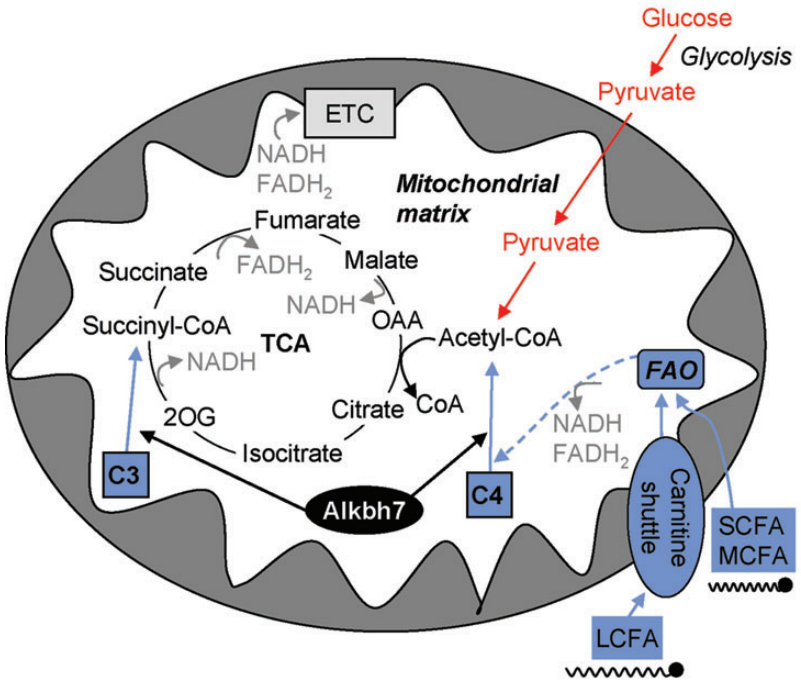

Figure 7 Model depicting the proposed role of Alkbh7 in the mitochondria. In this model, Alkbh7 facilitates the entry of the short-chain acylcarnitine species C3 and C4 into the TCA cycle. During fasting, the reliance on fatty acids as energy substrate is increased and fatty acids are catabolized via β-oxidation to produce NADH, $FADH_2$, and acetyl-CoA. We propose that Alkbh7 either directly or indirectly regulates the conversion of C3 and C4 acylcarnitines to succinyl-CoA and acetyl-CoA, leading to a number of downstream effects in the *Alkbh7*$^{-/-}$ mice. NADH, nicotinamide adenine dinucleotide (reduced form); $FADH_2$, flavin adenine dinucleotide (reduced form); OAA, oxaloacetic acid; CoA, coenzyme A; FAO, fatty acid oxidation; LCFA, long-chain fatty acid; MCFA, medium-chain fatty acid; SCFA, short-chain fatty acid; C3, C3 acylcarnitine (propionyl-CoA); C4 acylcarnitine (butyryl-CoA); 2OG, 2-oxoglutarate; TCA, tricarboxylic acid cycle; ETC, electron transport chain.

and C4 acylcarnitines in fasting *Alkbh7*$^{-/-}$ mice suggests that Alkbh7 is directly or indirectly involved in the metabolism of these acylcarnitines. Furthermore, we suggest that the *Alkbh7*$^{-/-}$ mice compensate for the reduced oxidation of C3 and C4 acylcarnitines during fasting by storing glycogen at levels that are much higher than their wild-type counterparts. Consistent with this, the strong mitochondrial substrate preference for pyruvate and glutamate in the *Alkbh7*$^{-/-}$ mouse indicates that these mice have adapted a preference for carbohydrates as an energy source. Furthermore, the fasting acylcarnitine profile partially explains the amplified obesity phenotype when the *Alkbh7*$^{-/-}$ mice were placed on an HFD as the HFD mimics fasting where the availability of carbohydrates is limited.

The deletion of *Alkbh7* has several downstream effects that could result from the increased fat mass and adipocyte size in the *Alkbh7*$^{-/-}$ mice. *Alkbh7*$^{-/-}$ plasma displays elevated levels of the adipocyte secreted appetite suppressing hormone leptin, which may explain the reduced food intake by the *Alkbh7*$^{-/-}$ mice compared with wild-type mice. Sustained, elevated leptin levels from increased adipose stores typically result in leptin desensitization causing an inability to suppress appetite (Borges et al., 2011). However, *Alkbh7*$^{-/-}$ mice do not appear to show this characteristic of leptin resistance as they eat less than wild-type mice when fed an HFD. We suggest that the altered energy substrate preference in the *Alkbh7*$^{-/-}$ mitochondria influences downstream signaling mechanisms and molecules that control the eating behavior in the *Alkbh7*$^{-/-}$ mice. A comprehensive analysis of the energy phenotype, including indirect calorimetry measurements that identify the basal metabolic rate and substrate preference, will be pursued in future experiments to elucidate the origin of the obesity phenotype in the *Alkbh7*$^{-/-}$ mice.

Another downstream effect we expected from the increased fat mass and adipocyte size was type 2 diabetes, as glucose intolerance and insulin resistance are strongly associated with obesity (Jain et al., 2012). Surprisingly, our data indicate that the deletion of *Alkbh7* protects these mice from HFD-induced glucose intolerance and insulin resistance in the female *Alkbh7*$^{-/-}$ mice. Several mouse models of obesity and diabetes have demonstrated gender-specific differences believed to be the result of a protective effect of certain female sex hormones (Gui et al., 2004; Macotela et al., 2009). Therefore, our results showing sex dependence for insulin sensitivity and glucose tolerance in the *Alkbh7*$^{-/-}$ mice could be expected.

In Figure 7, we propose a model in which Alkbh7 acts directly or indirectly in the conversion of C3 and C4 acylcarnitines to metabolites that are fed directly into the TCA cycle. While *Alkbh7*$^{-/-}$ mice show a buildup of the short-chain fatty acids C3 and C4 during fasting, β-oxidation of long- and medium-chain fatty acids still provides electrons to the electron transport chain for ATP production as well as acetyl-CoA for the TCA cycle. The derivation of energy from β-oxidation of long- and medium-chain fatty acids could explain why the *Alkbh7*$^{-/-}$ phenotype is not as severe as the effects observed in other fatty acid oxidation mouse models (Ibdah et al., 2001; Nyman et al., 2005; Ji et al., 2008). Interestingly, the deletion

of the ninth mouse AlkB homologue—Fto—results in reduced body weight, while the overexpression of Fto has been shown to cause obesity in mice (Church et al., 2009, 2010; Fischer et al., 2009). FTO is known to function as a nucleic acid demethylase (Gerken et al., 2007; Jia et al., 2008, 2011). However, the mechanism by which Fto affects obesity remains unclear. In contrast to the mitochondrial localization of the Alkbh7 protein, FTO localizes to the nucleus (Gerken et al., 2007). It is tempting to speculate that Alkbh7 and FTO have evolved in separate cellular compartments to have dissimilar mechanisms but have similar roles related to metabolism and energy use.

In summary, we demonstrate that deleting *Alkbh7* in mice results in abnormally high body fat levels, indicating that *Alkbh7* has a role in fat metabolism. We show that Alkbh7 resides in the mitochondrial matrix and suggest that altered fatty acid oxidation in the *Alkbh7*$^{-/-}$ mice results in the excessive storage of glycogen and fat in these mice. The present study and future studies elucidating the role of Alkbh7 and the pathway(s) that involve Alkbh7 will unravel more of the molecular mechanisms causing metabolic disease and obesity.

Materials and methods

Animal studies

Mice were housed in a virus-free facility at 22°C with a controlled 12 h light cycle. The mice were fed either an SD with 5.5% fat content (Rat and Mouse No. 3 breeding diet, Special Diet Services) or, when indicated, an HFD with 45% fat content (Research Diets) *ad libitum*. All mice in this study were C57BL/6J background strain homozygous *Alkbh7*$^{-/-}$ mice or wild-type mice. All SD data were obtained from 4-month-old mice. The mice used to acquire data for the SD were the same individuals that the HFD data were derived from. All experimental procedures were approved by the Section for Comparative Medicine at the Oslo University Hospital and the Norwegian Animal Research Authority, and comply with National laws and institutional regulations governing the use of animals in research.

RNA analysis

RNA was extracted from the respective tissues using Trizol Reagent as described by the manufacturer (Life Technologies). Two micrograms of RNA was reverse transcribed to cDNA using a high capacity RNA to cDNA kit (Applied Biosystems) according to the manufacturer's instructions. For each reaction, 0.25 ng cDNA was used with SYBR green probes (Life Technologies) and the quantities were normalized to glyceraldehyde-3-phosphate dehydrogenase (GAPDH) cDNA levels. All reactions were run on the Applied Biosystems Real-Time PCR System using the $\Delta\Delta C_T$ method (Schmittgen and Livak, 2008). The primers used are listed in Supplementary Table S1.

Antibodies

Primary antibodies. The polyclonal rabbit anti-Alkbh7 (6 μg/μl, western blotting 1:1000; IF 1:50) was custom made by Millipore using full length Alkbh7 protein as an antigen. Mouse anti-complex IV was used as a mitochondrial marker and a mitochondrial inner membrane marker for western blotting (Life Technologies, 1:1000). Mouse anti-cytochrome C was used as a mitochondrial marker for cellular localization (Life Technologies, IF 1:200). Rabbit PCNA (Abcam, western blotting 1:1000) was used as a nuclear marker. Rabbit anti-β-actin was used as a cytosolic marker (Abcam, western blotting 1:4000). Mouse anti-Hsp60 (Santa Cruz, western blotting 1:500) was used as a mitochondrial matrix marker. All antibodies were diluted in 0.5% blocking solution (Roche) and incubated overnight at 4°C.

Secondary antibodies. Horseradish peroxidase (HRP) conjugated secondary antibodies were used for western blot analysis at the following dilutions: Anti-rabbit IgG, 1:30000 (Sigma); Anti-mouse IgG, 1:30000 (Abcam). Fluorescence conjugated secondary antibodies were used at the following dilutions: Anti-rabbit IgG Alexa 488, 1:400 (Life Technologies); Anti-mouse IgG Alexa 594, 1:400 (Life Technologies). HRP conjugated antibodies were incubated with the western blot for 1 h at room temperature. Fluorescence conjugated antibodies were incubated with the cells for 30 min at room temperature.

Sub-cellular fractionation

Pure mitochondrial heart extracts were obtained as previously described (Wieckowski et al., 2009). Mitochondrial sub-fractionation was performed as previously described (Rardin et al., 2008).

Histological analysis of white adipose tissue

Paraffin embedded white adipose tissues were cut into 4.5 μm sections using a microtome (Thermo Scientific). Tissue sections were hematoxylin/eosin stained following standard procedures (Dries, 2008). Images of sections were captured using an AxioCam MR Rev3 camera on an Axio Observer microscope (Carl Zeiss) equipped with an AxioCam ICc1 camera (Carl Zeiss). The number and size of the white adipose cells were counted and measured using the AxioVision 4.8 software (Carl Zeiss) and the Cell Counter program in ImageJ software (Abramoff et al., 2004). The adipocyte size was measured as fiber length by micrometer per pixel defined by the Axiovision software. A line was drawn from one end of the adipose cell to the end furthest away from the starting point and ImageJ calculated the length of this line defined by the set micrometer per pixel. The sizes of at least 300 white adipose cells were measured per adipose section.

Serum analysis

Serum glucose levels were measured using the Freestyle Lite blood glucose monitoring system (Abbott Laboratories). Serum insulin levels were measured using an Ultra Sensitive Mouse Insulin ELISA kit (Crystal Chem, Inc.). Serum total cholesterol, triglyceride, HDL (high-density lipoprotein) cholesterol, and LDL (low-density lipoprotein) cholesterol levels were measured using a CardioCheck PA analyzer and Lipidpanel strips (MedCam AB). The lipid status was determined by the CardioCheck PA analyzer using one drop of blood from the hind leg vein after overnight fasting. Plasma leptin and adiponectin levels were determined by a Mouse Leptin ELISA kit (Crystal Chem, Inc.) and an Adiponectin Mouse ELISA kit (Biovision, Inc.), respectively. β-hydroxybutyrate was measured with a β-hydroxybutyrate kit from Biovision, Inc. Insulin tolerance was measured using an insulin tolerance test (ITT); mice were fasted 5 h before intraperitoneal (i.p.) injection with 0.75 U Humalog insulin (Eli Lilly & Co.) per kilogram of body weight. For the glucose tolerance test (GTT), mice were fasted 16 h before i.p. injection with 2 g of D-(+)-glucose (Sigma) per kilogram of body weight. The glucose levels were determined prior to injection ($t = 0$) and at the indicated times after injection of either insulin or glucose. Approximately 50 μl of blood sample was left at room temperature for 1 h to coagulate and then plasma was

separated twice by centrifugation at 2000 *g* for 10 min at 4°C and frozen for later use in an ELISA.

Glycogen levels

Glycogen levels were measured in 10 mg liver extract from overnight fasting female mice on an SD according to the instructions of the glycogen assay kit from Biovision.

Food intake and body composition

Food intake was measured in metabolic cages for single mouse housing (Scanbur). The mice were housed in the metabolic cages for 24 h at the beginning of the HFD ($t = 0$), after 2 weeks on HFD, after 1 month on HFD, and when the HFD was finished (after 8 weeks). The mice were acclimatized for 24 h prior to all food intake measurements, which were done after 24 h housing in the metabolic cages and calculated as mass chow consumed per 24 h per unit mass of body weight. Body composition (fat and lean content) was determined by dual-energy X-ray absorptiometry using a DEXA Lunar PIXImus Densitometer (GE Healthcare). The mice were anesthetized by i.p. injection of 0.1 ml per 20 g body weight of Hypnorm/Dormicum (1.25 mg/ml Dormicum, 2.5 mg/ml fluanisone, 0.079 mg/ml fentanyl citrate) to acquire the X-ray images. The analysis of lean mass and fat mass was performed using a region of interest comprising from the start of the tail to the start of the ribcage (near the diaphragm), as the mice were too big to fit the entire body in the image area.

Physical activity

Open field tests to measure voluntary physical activity were conducted using a VersaMax animal activity monitoring system (AccuScan Instruments) according to the manufacturer's instructions. The results are presented as the number of beam breaks per 15 min. Two mice were measured simultaneously in separate compartments and the data were analyzed using the VersaDat software (AccuScan Instruments).

Mitochondrial respiration

Mitochondrial respiration was studied *in situ* in saponin permeabilized cardiac fibers as previously described (Kuznetsov et al., 2008). Briefly, the maximal fiber respiration rates were measured at 22°C under continuous stirring in the presence of saturating amount of 2 mM ADP as phosphate acceptor together with 20 mM creatine in a 3 ml water-jacketed oxygraphic cell equipped with a Clark electrode (Strathkelvin Instruments). Four millimolar malate was added to the reaction and respiration was monitored after the addition of substrates in the following order: 135 μM palmitoyl-carnitine, 1 mM pyruvate, 10 mM glutamate, and 10 mM succinate. After the experiment, fibers were harvested and dried and respiration rates were expressed as micromoles of O_2 per minute per gram dry weight.

Acylcarnitine and amino acid profiling

Metabolomic analyses were performed at the Metabolomics Innovation Centre (University of Alberta, Canada) using a targeted quantitative metabolomics approach of combined direct flow injection and liquid chromatography MS/MS (AbsolutIDQ™ p180 kit, Biocrates Life Sciences AG). The AbsolutIDQ™ p180 kit (Biocrates Life Sciences AG), in combination with a 4000 QTrap mass spectrometer (Applied Biosystems/MDS Sciex), allowed simultaneous quantification of 157 metabolites (including 23 acylcarnitines and 20 amino acids). The method combines the derivatization and extraction of analytes with the selective mass-spectrometric detection using multiple reaction monitoring (MRM) pairs. Isotope-labeled internal standards are integrated into a kit plate filter for metabolite quantification. A total of 10 μl of supernatant from each serum sample from female mice was loaded on a filter paper placed on top of the kit plate and dried in a stream of nitrogen. Subsequently, 20 μl of a 5% solution of phenyl-isothiocyanate was added for derivatization. After incubation, the filter spots were dried again using an evaporator. Extraction of the metabolites was then achieved by adding 300 μl methanol containing 5 mM ammonium acetate. The extracts were obtained by centrifugation into the lower 96-deep-well plate, followed by a dilution step with 600 μl of the kit's mass spectrometry running solvent.

Statistical analysis

All data are presented as mean ± standard error of the means (SEM), unless otherwise stated in the text. Statistical significance was determined using an unpaired two-tailed Student's *t*-test. Statistical significance was defined as $P < 0.05$. $^{*}P < 0.05$, $^{**}P < 0.01$, $^{***}P < 0.001$. Statistical analysis was performed using the GraphPad Prism version 5.04 software.

Note added in proof

While this paper was in review, complementary data on the mitochondrial targeting of ALKBH7, and a role for human ALKBH7 for programmed necrosis was published (Dragony, F., Jordan, J.J., and Samson, L.D. (2013) Human ALKBH7 is required for alkylation and oxidation-induced programmed necrosis, Genes & Development, in press).

Supplementary material

Supplementary material is available at *Journal of Molecular Cell Biology* online.

Acknowledgements

We thank GenOway (Lyon, France), the Norwegian Transgenic Center and Center for Comparative studies at Oslo University Hospital HF for excellent service. We are grateful to Prof. L. Nordsletten and Prof. K.M. Gautvik at Oslo University Hospital HF for the use of the PIXImus apparatus, and H. Wixen and G.F. Lien at Oslo University Hospital HF for their assistance with the mice and tissue sectioning.

Funding

This work was supported by Oslo University Hospital, and the FRIBIO and FUGE programs provided by the Research Council of Norway and the Norwegian Cancer Society.

Conflict of interest: None declared.

References

Abramoff, M.D., Magahaes, P.J., and Ram, S.J. (2004). Image processing with Image. J. Biophotonics Int. *11*, 36–42.

Aravind, L., and Koonin, E.V. (2001). The DNA-repair protein AlkB, EGL-9, and leprecan define new families of 2-oxoglutarate- and iron-dependent dioxygenases. Genome Biol. *2*, RESEARCH0007.

Berulava, T., Ziehe, M., Klein-Hitpass, L., et al. (2013). FTO levels affect RNA modification and the transcriptome. Eur. J. Hum. Genet. *21*, 317–323.

Borges, B.C., Rorato, R., Avraham, Y., et al. (2011). Leptin resistance and desensitization of hypophagia during prolonged inflammatory challenge. Am. J. Physiol. Endocrinol. Metab. *300*, E858–E869.

Bray, M.S., Tsai, J.Y., Villegas-Montoya, C., et al. (2010). Time-of-day-dependent dietary fat consumption influences multiple cardiometabolic syndrome parameters in mice. Int. J. Obes. *34*, 1589–1598.

Church, C., Lee, S., Bagg, E.A., et al. (2009). A mouse model for the metabolic effects of the human fat mass and obesity associated FTO gene. PLoS Genet. *5*, e1000599.

Church, C., Moir, L., McMurray, F., et al. (2010). Overexpression of Fto leads to increased food intake and results in obesity. Nat. Genet. *42*, 1086–1092.

Claros, M.G., and Vincens, P. (1996). Computational method to predict mitochondrially imported proteins and their targeting sequences. Eur. J. Biochem. *241*, 779–786.

Coll, A.P., Farooqi, I.S., and O'Rahilly, S. (2007). The hormonal control of food intake. Cell *129*, 251–262.

Dango, S., Mosammaparast, N., Sowa, M.E., et al. (2011). DNA unwinding by ASCC3 helicase is coupled to ALKBH3-dependent DNA alkylation repair and cancer cell proliferation. Mol. Cell *44*, 373–384.

Dina, C., Meyre, D., Gallina, S., et al. (2007). Variation in FTO contributes to childhood obesity and severe adult obesity. Nat. Genet. *39*, 724–726.

Dries, D.J. (2008). Histological and histochemical methods: theory and practice, 4th edition. Shock *30*, 481.

Duncan, T., Trewick, S.C., Koivisto, P., et al. (2002). Reversal of DNA alkylation damage by two human dioxygenases. Proc. Natl Acad. Sci. USA *99*, 16660–16665.

Falnes, P.O., Johansen, R.F., and Seeberg, E. (2002). AlkB-mediated oxidative demethylation reverses DNA damage in Escherichia coli. Nature *419*, 178–182.

Fischer, J., Koch, L., Emmerling, C., et al. (2009). Inactivation of the Fto gene protects from obesity. Nature *458*, 894–898.

Frayling, T.M., Timpson, N.J., Weedon, M.N., et al. (2007). A common variant in the FTO gene is associated with body mass index and predisposes to childhood and adult obesity. Science *316*, 889–894.

Frederich, R.C., Hamann, A., Anderson, S., et al. (1995). Leptin levels reflect body lipid content in mice: evidence for diet-induced resistance to leptin action. Nat. Med. *1*, 1311–1314.

Fu, Y., Dai, Q., Zhang, W., et al. (2010). The AlkB domain of mammalian ABH8 catalyzes hydroxylation of 5-methoxycarbonylmethyluridine at the wobble position of tRNA. Angew. Chem. Int. Ed. *49*, 8885–8888.

Gerken, T., Girard, C.A., Tung, Y.C., et al. (2007). The obesity-associated FTO gene encodes a 2-oxoglutarate-dependent nucleic acid demethylase. Science *318*, 1469–1472.

Gui, Y., Silha, J.V., and Murphy, L.J. (2004). Sexual dimorphism and regulation of resistin, adiponectin, and leptin expression in the mouse. Obes. Res. *12*, 1481–1491.

Haynes, C.A. (2011). Analysis of mammalian fatty acyl-coenzyme A species by mass spectrometry and tandem mass spectrometry. Biochim. Biophys. Acta *1811*, 663–668.

Hetherington, M.M., and Cecil, J.E. (2010). Gene-environment interactions in obesity. Forum Nutr. *63*, 195–203.

Ibdah, J.A., Paul, H., Zhao, Y., et al. (2001). Lack of mitochondrial trifunctional protein in mice causes neonatal hypoglycemia and sudden death. J. Clin. Invest. *107*, 1403–1409.

Jain, D., Jain, R., Eberhard, D., et al. (2012). Age- and diet-dependent requirement of DJ-1 for glucose homeostasis in mice with implications for human type 2 diabetes. J. Mol. Cell Biol. *4*, 221–230.

Ji, S., You, Y., Kerner, J., et al. (2008). Homozygous carnitine palmitoyltransferase 1b (muscle isoform) deficiency is lethal in the mouse. Mol. Genet. Metab. *93*, 314–322.

Jia, G., Yang, C.G., Yang, S., et al. (2008). Oxidative demethylation of 3-methylthymine and 3-methyluracil in single-stranded DNA and RNA by mouse and human FTO. FEBS Lett. *582*, 3313–3319.

Jia, G., Fu, Y., Zhao, X., et al. (2011). N6-Methyladenosine in nuclear RNA is a major substrate of the obesity-associated FTO. Nat. Chem. Biol. *7*, 885–887.

Kahn, S.E., Hull, R.L., and Utzschneider, K.M. (2006). Mechanisms linking obesity to insulin resistance and type 2 diabetes. Nature *444*, 840–846.

Kataoka, H., Yamamoto, Y., and Sekiguchi, M. (1983). A new gene (alkB) of Escherichia coli that controls sensitivity to methyl methane sulfonate. J. Bacteriol. *153*, 1301–1307.

Kelly, T., Yang, W., Chen, C.S., et al. (2008). Global burden of obesity in 2005 and projections to 2030. Int. J. Obes. (Lond) *32*, 1431–1437.

Kurowski, M.A., Bhagwat, A.S., Papaj, G., et al. (2003). Phylogenomic identification of five new human homologs of the DNA repair enzyme AlkB. BMC Genomics *4*, 48.

Kuznetsov, A.V., Veksler, V., Gellerich, F.N., et al. (2008). Analysis of mitochondrial function in situ in permeabilized muscle fibers, tissues and cells. Nat. Protoc. *3*, 965–976.

Larder, R., Cheung, M.K., Tung, Y.C., et al. (2011). Where to go with FTO? Trends Endocrinol. Metab. *22*, 53–59.

Ma, S., Yu, H., Zhao, Z., et al. (2012). Activation of the cold-sensing TRPM8 channel triggers UCP1-dependent thermogenesis and prevents obesity. J. Mol. Cell Biol. *4*, 88–96.

Macotela, Y., Boucher, J., Tran, T.T., et al. (2009). Sex and depot differences in adipocyte insulin sensitivity and glucose metabolism. Diabetes *58*, 803–812.

McMurray, F., Church, C.D., Larder, R., et al. (2013). Adult onset global loss of the fto gene alters body composition and metabolism in the mouse. PLoS Genet. *9*, e1003166.

Nordstrand, L.M., Svard, J., Larsen, E., et al. (2010). Mice lacking Alkbh1 display sex-ratio distortion and unilateral eye defects. PLoS One *5*, e13827.

Nyman, L.R., Cox, K.B., Hoppel, C.L., et al. (2005). Homozygous carnitine palmitoyltransferase 1a (liver isoform) deficiency is lethal in the mouse. Mol. Genet. Metab. *86*, 179–187.

Ougland, R., Lando, D., Jonson, I., et al. (2012). ALKBH1 is a histone H2A dioxygenase involved in neural differentiation. Stem Cells *30*, 2672–2682.

Pan, Z., Sikandar, S., Witherspoon, M., et al. (2008). Impaired placental trophoblast lineage differentiation in Alkbh1(−/−) mice. Dev. Dyn. *237*, 316–327.

Rardin, M.J., Wiley, S.E., Murphy, A.N., et al. (2008). Dual specificity phosphatases 18 and 21 target to opposing sides of the mitochondrial inner membrane. J. Biol. Chem. *283*, 15440–15450.

Ringvoll, J., Nordstrand, L.M., Vagbo, C.B., et al. (2006). Repair deficient mice reveal mABH2 as the primary oxidative demethylase for repairing 1meA and 3meC lesions in DNA. EMBO J. *25*, 2189–2198.

Ringvoll, J., Moen, M.N., Nordstrand, L.M., et al. (2008). AlkB homologue 2-mediated repair of ethenoadenine lesions in mammalian DNA. Cancer Res. *68*, 4142–4149.

Schmittgen, T.D., and Livak, K.J. (2008). Analyzing real-time PCR data by the comparative CT method. Nat. Protoc. *3*, 1101–1108.

Songe-Moller, L., van den Born, E., Leihne, V., et al. (2010). Mammalian ALKBH8 possesses tRNA methyltransferase activity required for the biogenesis of multiple wobble uridine modifications implicated in translational decoding. Mol. Cell. Biol. *30*, 1814–1827.

Sovio, U., Mook-Kanamori, D.O., Warrington, N.M., et al. (2011). Association between common variation at the FTO locus and changes in body mass index from infancy to late childhood: the complex nature of genetic association through growth and development. PLoS Genet. *7*, e1001307.

Stratigopoulos, G., and Leibel, R.L. (2010). FTO gains function. Nat. Genet. *42*, 1038–1039.

Trewick, S.C., Henshaw, T.F., Hausinger, R.P., et al. (2002). Oxidative demethylation by Escherichia coli AlkB directly reverts DNA base damage. Nature *419*, 174–178.

Tsujikawa, K., Koike, K., Kitae, K., et al. (2007). Expression and sub-cellular localization of human ABH family molecules. J. Cell. Mol. Med. *11*, 1105–1116.

van den Born, E., Vagbo, C.B., Songe-Moller, L., et al. (2011). ALKBH8-mediated formation of a novel diastereomeric pair of wobble nucleosides in mammalian tRNA. Nat. Commun. *2*, 172.

Wang, S., Yehya, N., Schadt, E.E., et al. (2006). Genetic and genomic analysis of a fat mass trait with complex inheritance reveals marked sex specificity. PLoS Genet. *2*, e15.

Wei, Y.F., Carter, K.C., Wang, R.P., et al. (1996). Molecular cloning and functional analysis of a human cDNA encoding an Escherichia coli AlkB homolog, a protein involved in DNA alkylation damage repair. Nucleic Acids Res. *24*, 931–937.

Wieckowski, M.R., Giorgi, C., Lebiedzinska, M., et al. (2009). Isolation of mitochondria-associated membranes and mitochondria from animal tissues and cells. Nat. Protoc. *4*, 1582–1590.

Zheng, G., Dahl, J.A., Niu, Y., et al. (2013). ALKBH5 is a mammalian RNA demethylase that impacts RNA metabolism and mouse fertility. Mol. Cell *49*, 18–29.